Supplementary Material for

Low Fatigue Dynamic Auxetic Lattices with 3D Printable, Multistable, and Tuneable Unit Cells

Eesha Khare[1], Stephen Temple[1], Ivan Tomov[1], Fenghua Zhang[1,2], Stoyan K. Smoukov[1,3]*

[1]Active and Intelligent Materials Lab, Department of Materials Science and Metallurgy, University of Cambridge, Cambridge UK
[2]Centre for Composite Materials and Structures, Harbin Institute of Technology, Harbin, China
[3]School of Engineering and Materials Science, Queen Mary University of London, London UK

*** Correspondence:** Stoyan Smoukov; s.smoukov@qmul.ac.uk

Supplementary Information

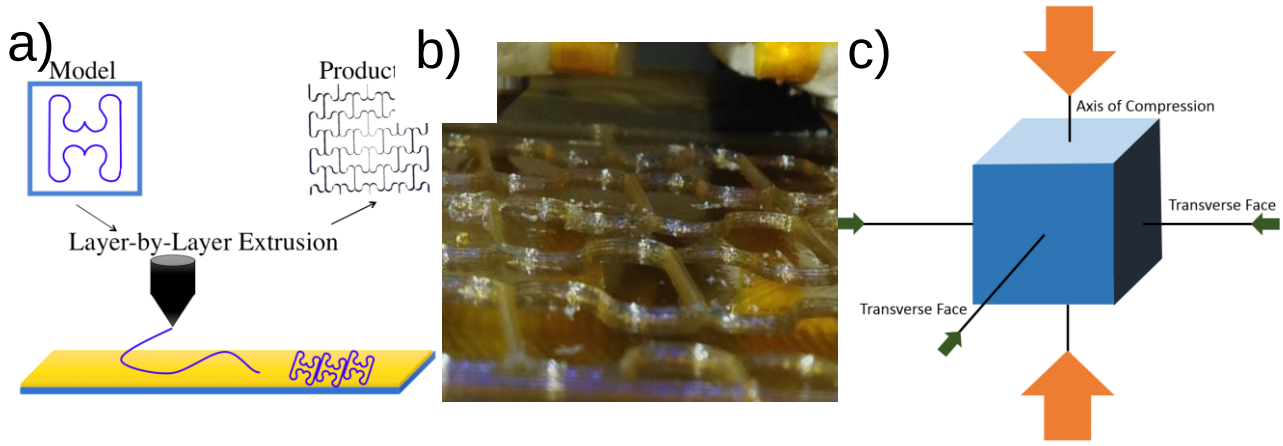

Supplementary Figure S1. a) Rapid 3D printing enabled the fabrication of s-hinged unit cell into 2D and 3D auxetic structures. b) MakerBot Replicator layer-by-layer 3D printing. c) Diagram depicting compression behavior of auxetic. When compressed along the axis of compression (marked in orange arrows), the transverse faces marked in green contract inwards

Experimental and Finite Element Models

Supplementary Figure S2 demonstrates that there is good agreement between the finite element simulation and experimental force-displacement data for the rigid rib direction of the conventional honeycomb and s-hinge auxetic in the elastic region of the structures. It is important to note that the finite element models only take into account the elastic properties of the materials, so the simulations are only expected to be accurate for the elastic region of the curves, until the compressive strength of PLA is exceeded.

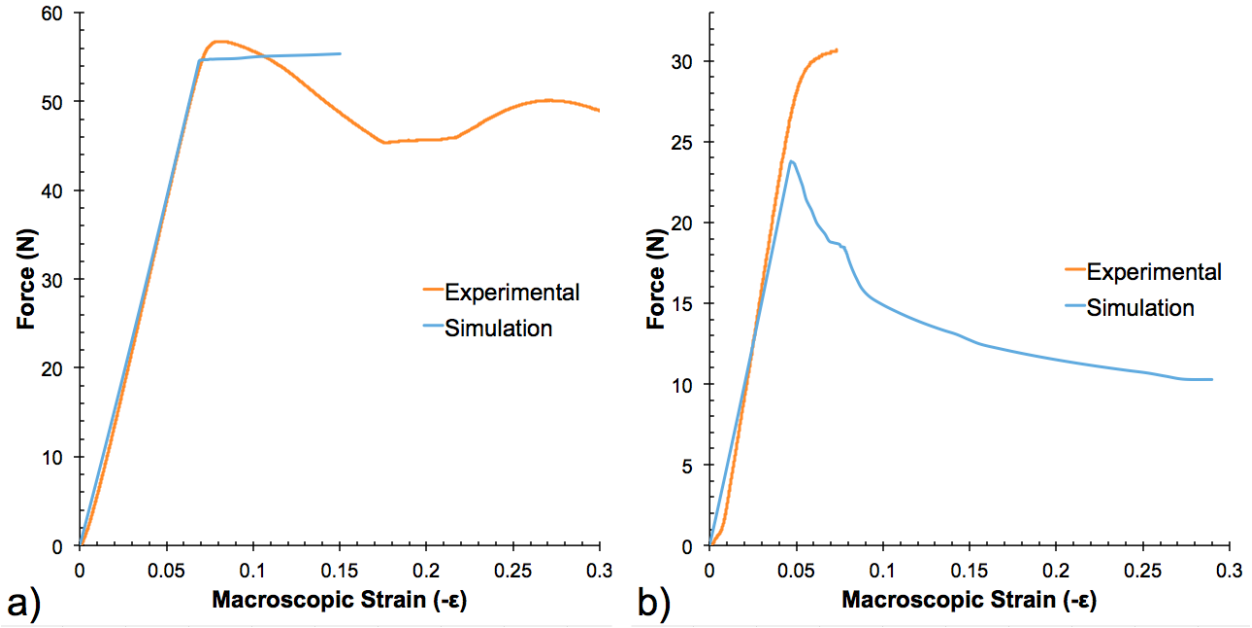

Supplementary Figure S1. Comparison of simulation and experimental data for compression in the rib direction for the (a) conventional honeycomb and (b) s-hinge auxetic.

Analysis of Equivalent Plastic Strain

Supplementary Figure S3 demonstrates the equivalent local plastic strain upon 9.5% macroscopic deformation of the structures. At this macroscopic deformation, the conventional honeycomb shows signs of plastic yielding, as some corners in the geometry begin to experience stresses higher than the compressive strength of PLA; in other words, the equivalent plastic strain in these regions is greater than zero. In contrast, the stresses in the s-hinged honeycomb do not exceed the compressive strength of PLA and thus do not plastically deform. In fact, plastic strains begin to occur only when the s-hinged structure is deformed to greater than 30.3% macroscopic strain. This result again demonstrates the benefit of increased elastic macroscopic deformation gained from the s-hinged structure.

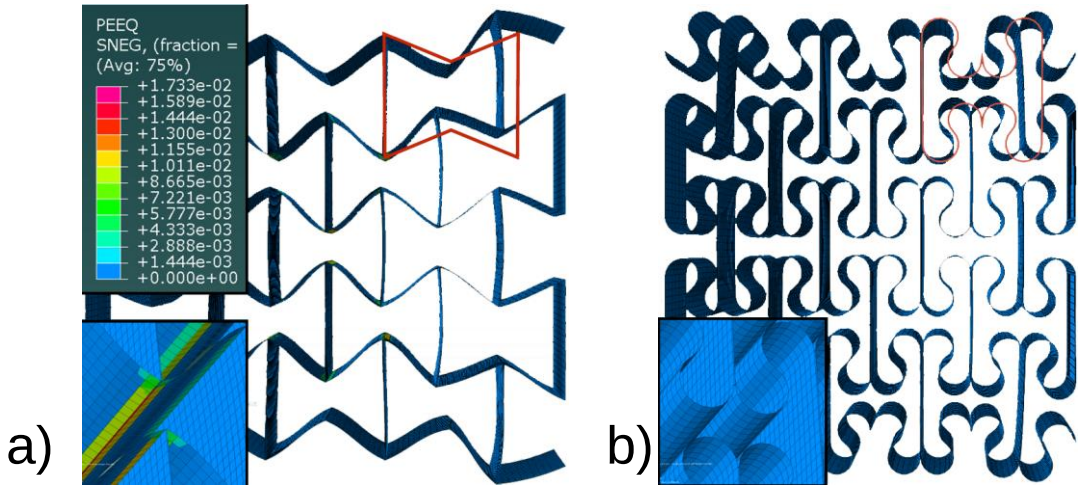

Fig. S3. Stress is in MPa and the orange outline represents the original undeformed cell. When deformed to 9.5% macroscopic strain, the conventional honeycomb begins to experience plastic deformation. Finite element analysis demonstrates that (a) equivalent plastic strain is greater than zero, signifying plastic deformation in the conventional honeycomb, and (b) it is zero in the s-hinged model.

1.1 Analysis of the Conventional Honeycomb Structure

To compare the 225 degree arc s-hinged auxetic to the re-entrant honeycomb from which it was derived, a re-entrant honeycomb was made with the same leg length and connecting angle as the s-hinge, as displayed in **Fig. 1a**. This comparative honeycomb was characterized by determining force versus displacement curves when loaded in different directions. Both when deformed along the rigid ribs and the hinges, the honeycomb illustrates an elastic-plastic response, as demonstrated in **Fig. S4**. In both directions, the honeycomb exhibits an elastic region where it demonstrates auxetic property contracting in both directions as load is applied. When deformed along the rigid rib length, the honeycomb experiences a non-uniform shear sliding which results in a plastic buckling and collapse of the structure (Figure S4). In contrast, when deformed along the hinge direction, the honeycomb exhibits plane dislocations, much like the s-hinged structure when deformed along the direction of the hinges (Figure S4b). Once the honeycomb begins to experience this in-plane buckling, the local buckling stress exceeds the compressive strength of the PLA printed material, as demonstrated through finite element modeling, and thus this buckling correlates with plastic deformation of the structure. Progressive failure occurs unevenly along the structure, resulting in densification where additional contact points are made between the ribs and hinges. Note that the jagged peaks in Figure 4a are a result of the breaking of the corners in the hinge.

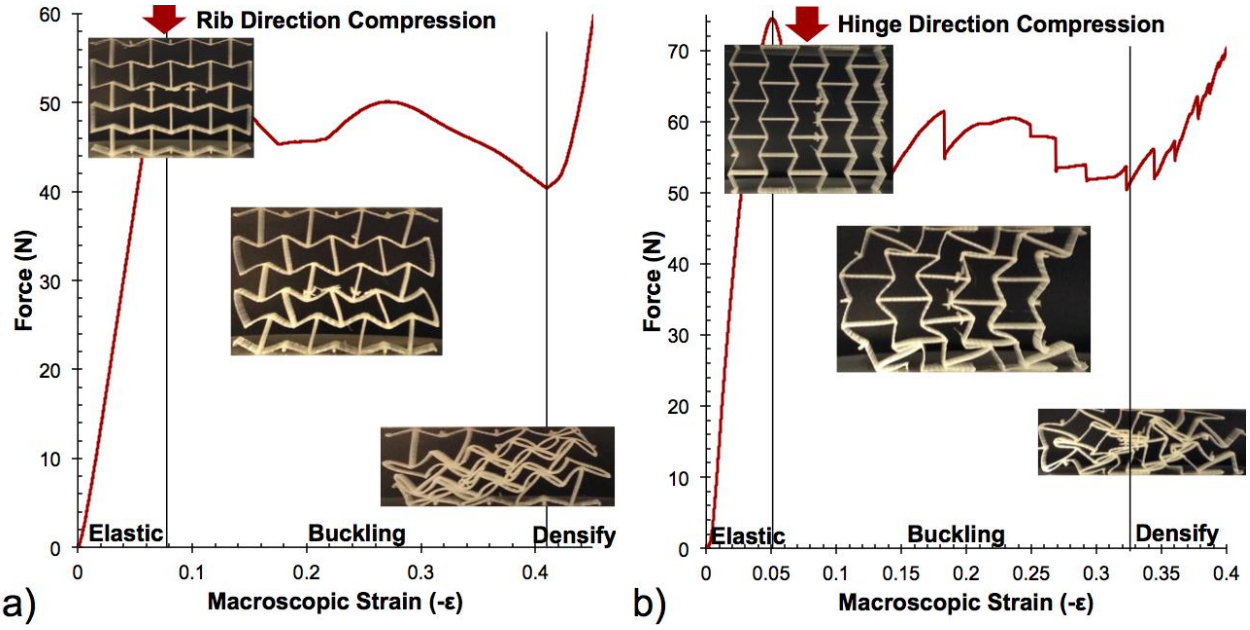

Fig. S4. Force-displacement characterization for conventional honeycomb. Deformation is depicted along the (a) rigid rib and (b) hinge direction.

1.2 Analysis of Similar S-hinge Auxetics

Force-displacement curves for similar s-hinged structures were also characterized. **Fig. S5** demonstrates this characterization for the s-hinged auxetic made from 180-degree arc. When deformed in both directions, the 180 degree arc s-hinged auxetic demonstrates the elastic-plateau-densification response. The auxetic property is demonstrated during the elastic region where the structure contracts inwards as it is being compressed. Like the conventional honeycomb and 225 degree arc s-hinged auxetic deformed along the hinge direction, the 180-degree arc s-hinged auxetic demonstrates a shearing or plane dislocation region. Unlike in the honeycomb however, this region is termed elastic buckling because the structure demonstrates near complete strain recovery after buckling. This is because stress is more evenly distributed through the hinges, just like in the 225-degree arc s-hinged auxetic. Therefore, the maximum stress is less likely to exceed the compressive strength of PLA. Unlike the 225-degree arc s-hinged auxetic, this structure demonstrates qualitative near-isotropic behavior when compressed in the rigid rib and hinge direction. This may be because of a number of factors that affect the deformation behavior of the s-hinged auxetic. These factors include the thickness of the beam and length of the rigid rib connecting the hinges. In this study, we use a constant rigid rib length and beam thickness for each sample. We change only the arc angle of the hinge. Perhaps changing these other aforementioned parameters will affect the deformation behavior of the auxetic; however, at present, this is beyond the scope of this work. Also, note that the sudden drop in Figure S5a is a result of the sudden inwards contraction of the structure because there is a small amount of friction along the surface of the plate that prevents the structure from neatly sliding inwards.

Force-displacement curves for double s-hinge structures with different arc angles were also characterized (**Fig. S6**). The positive Poisson's ratio 120-degree double s-hinge auxetic demonstrates a directly transition from elastic to densification regions when compressed in the rib direction, likely because the rigid ribs help guide the structure to prevent in-plane buckling (Fig. S6a). In contrast,

when compressed along the hinge direction, the structure exhibits in-plane buckling (Fig. S6b). At the critical angle of 140 degrees, we see similar behavior with direct transition along the rib direction (Fig. S6c) and in-plane buckling along the hinge direction (Fig. S6d).

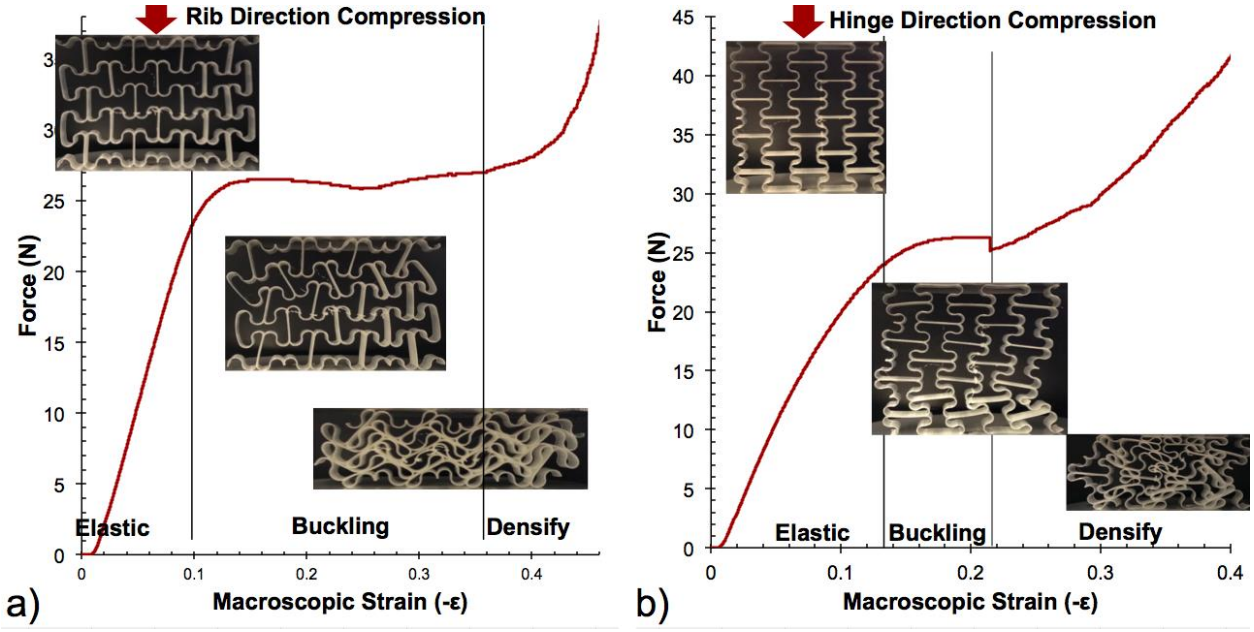

Fig. S5. Force-displacement characterization for 180-degree arc s-hinged auxetic. Note that this elastic region is much larger than that of the honeycomb. Deformation is depicted along the (a) rigid rib and (b) hinge direction.

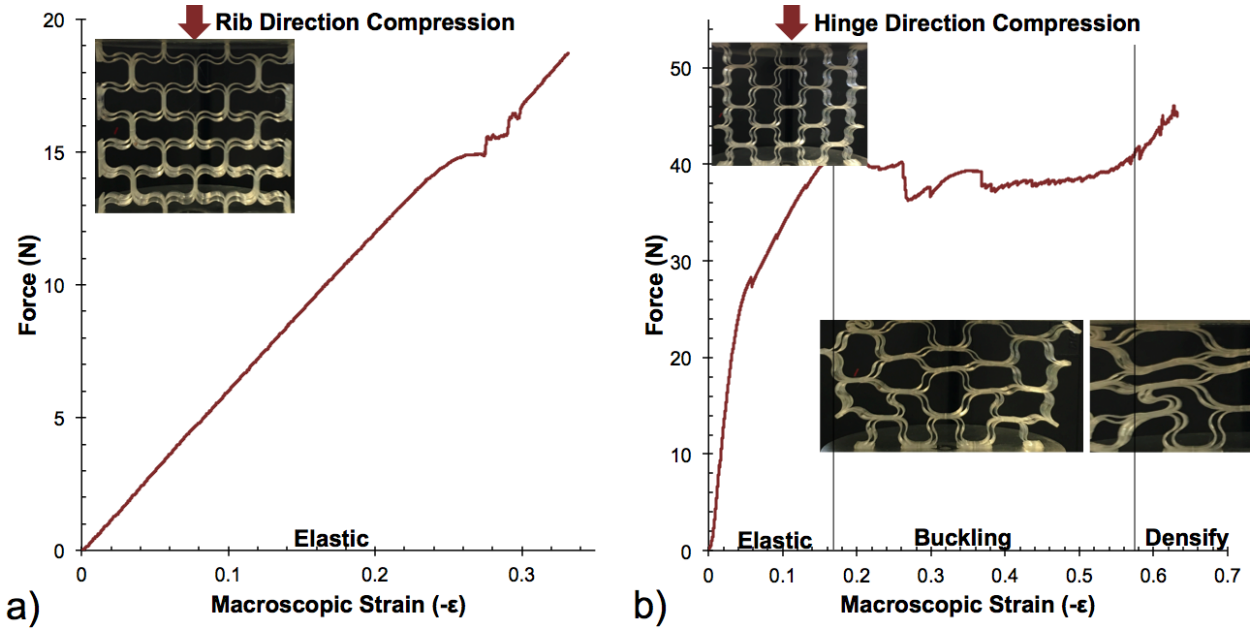

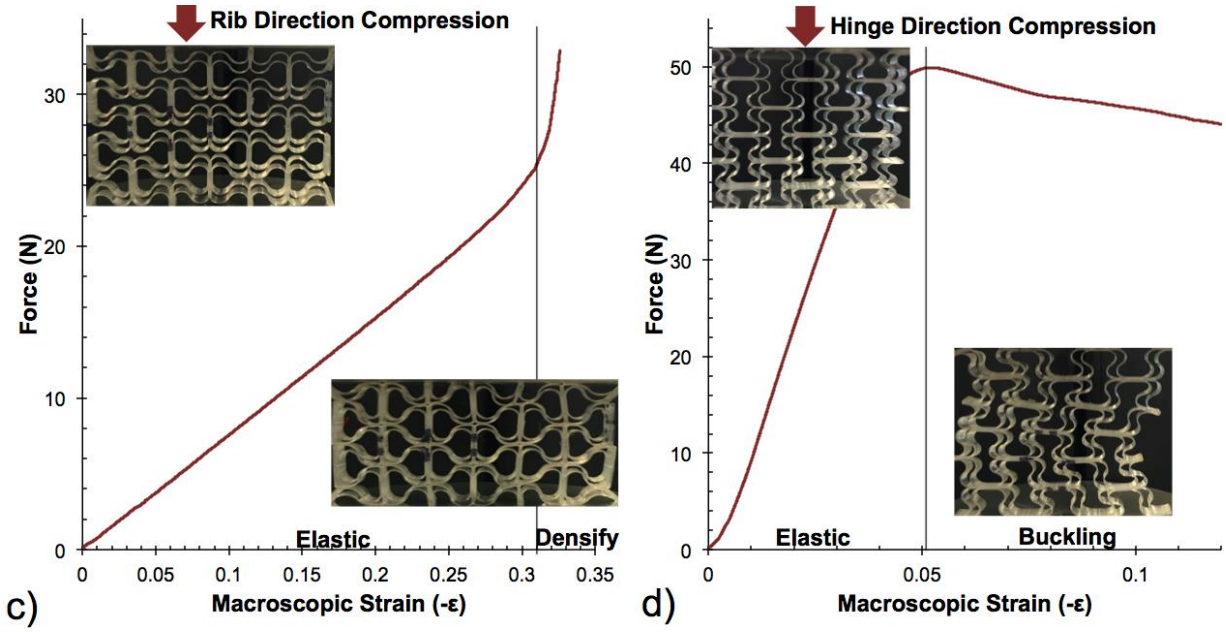

Fig. S6. Force-displacement characterization for 120-degree and 140-degree double s-hinge auxetic. When the 120-degree double hinge s-hinge auxetic is compressed in the (a) rib direction, it exhibits an elastic behavior. When compressed in the (b) hinge direction, it exhibits in-plane buckling. When the 140-degree double hinge s-hinge auxetic is compressed in the (c) rib direction, it exhibits no in-plane buckling and (d) hinge direction.

Analytical Modeling of S-Hinge

Bending stresses and strains are related by the fundamental equation of bending

$$\frac{M}{I} = \frac{E}{R} \tag{1}$$

where M is the applied bending moment, I is the second moment of area, and E is the Young's modulus of the material, and R is the radius of curvature of the beam.

In conventional analysis, the beam is assumed to be straight initially. However, for an initially curved beam, we must use the change in radius from the initial shape

$$\delta R = \frac{1}{\left(\frac{1}{R} - \frac{1}{R_0}\right)} \tag{2}$$

where R_o is the initial radius curvature and R is the subsequent radius of curvature.

Our analytical calculation is additionally complicated by the axial application of force. In conventional analysis, the beam experiences a transverse force. In our buckling calculations however, the axial force application results in a bending moment that depends upon the local deflected shape of the beam, yielding a complex relationship. These two conditions together—the initial curved structure and axially applied force—make a simple analytical solution difficult.

We implemented a semi-analytical parametric model in order to determine the force-displacement and Poisson's ratio of our s-hinged structures. The methods used in this semi-analytical model are applicable to a wider range of complex initial geometries and force applications. Using Microsoft Excel, we developed an iterative system of analytical formulas, which use the initial curved structure of the beam to calculate where it moves upon applying an incremental force.

The deflections of the beam can be calculated by using an intrinsic relationship between the length along the curved beam, *s*, and the tangential angle, α,

$$\frac{\delta s}{\delta \alpha} = R \tag{3}$$

By using an incremental form of this relationship, we can carry out a finite integration of the deflection of the beam and then iterate to find the appropriate fixed moments. The ends of the beam are constrained not to rotate, as in our physical model the hinges are constrained by the rigid ribs. Therefore, the fixed end moments are found by applying an incremental force less than 10% of the maximum compressive force

$$M_0 = -\left(\frac{Fy_i X_{i-1,n} + Fx_i Y_{i-1,n}}{2}\right) \tag{4}$$

where M_0 is the bending moment at the start of the curve, Fy is the force applied in the hinge direction, Fx is the force applied in the rib direction, X and Y are coordinates of the curve, and the primary index i represents the time step and the secondary index n represents the position along the curve. For the fixed end moments, n=1, the end position of the hinge.

Using the fixed end moments, moments along the remainder of the beam (M_n) are calculated.

$$M_{i,n} = M_0 + Fx_{i,n} Y_{i-1,n} + Fy_{i,n} X_{i-1,n} \tag{5}$$

These moments are used to calculate the resulting radius of curvature, R_n, and change in tangential angle, α_n.

$$R_{i,n} = \frac{1}{\left(\frac{1}{R_0} - \frac{M_{i,n}}{EI}\right)} \tag{6}$$

$$\delta\alpha_{i,n} = \frac{\delta s}{R_{i,n}} \tag{7}$$

The tangential angle is then used to determine the new position by stepping along the curve.

$$\alpha_{i,n+1} = \alpha_{i,n} + \delta\alpha_{i,n} \tag{8}$$

$$x_{i,n+1} = x_{i,n} + 2R_{i,n} tan\left(\frac{\delta\alpha_{i,n}}{2}\right) \cos(\alpha_{i,n}) \tag{9}$$

$$y_{i,n+1} = y_{i,n} + 2R_{i,n} tan\left(\frac{\delta\alpha_{i,n}}{2}\right) \sin(\alpha_{i,n}) \tag{10}$$

This process is repeated several times to yield the deformation of the hinge over several applied forces (Fig. 4a). Note that when the force was determined by $F_x = \mu F_y$, where μ is the measured coefficient of friction between the plates and printed structure, excellent agreement in the

force displacement curves was found. Further, the fact that the bending moment at the center of the curve must be zero by symmetry was used as a checkpoint in our calculations.

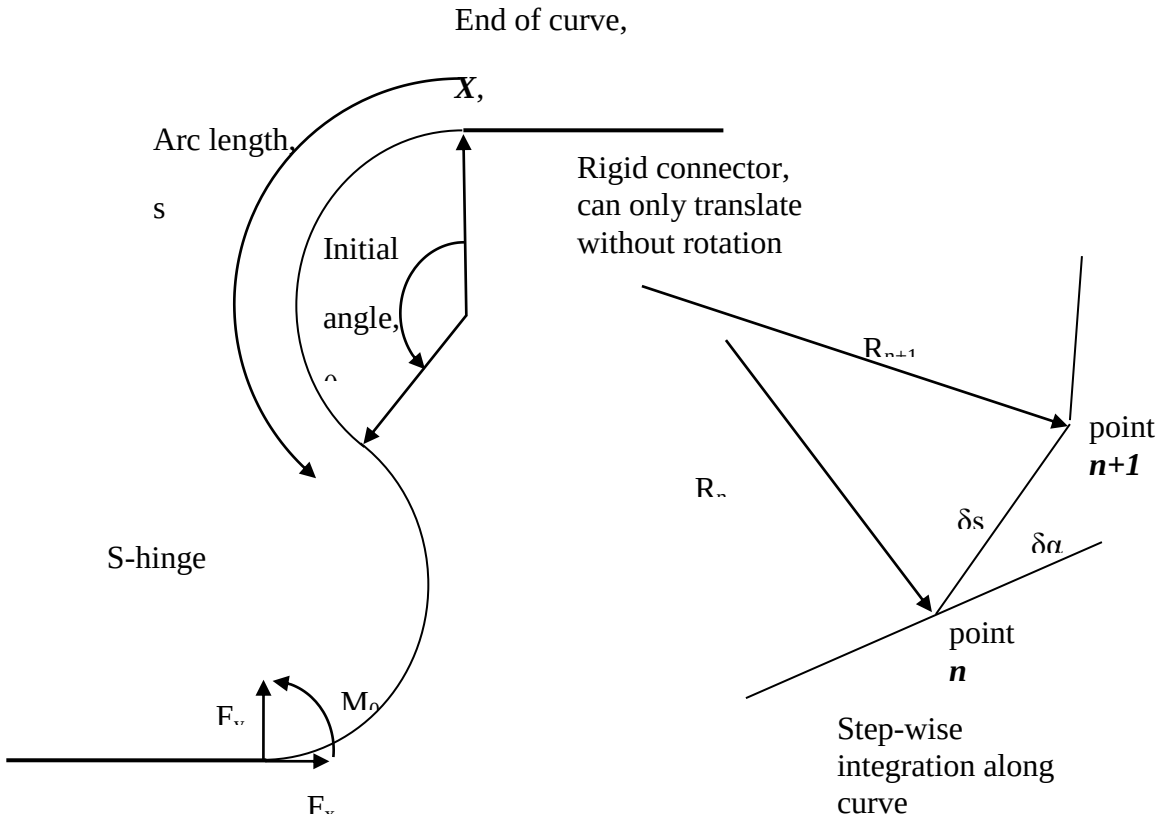

Figure S7. Schematic used for the semi-analytical calculation.

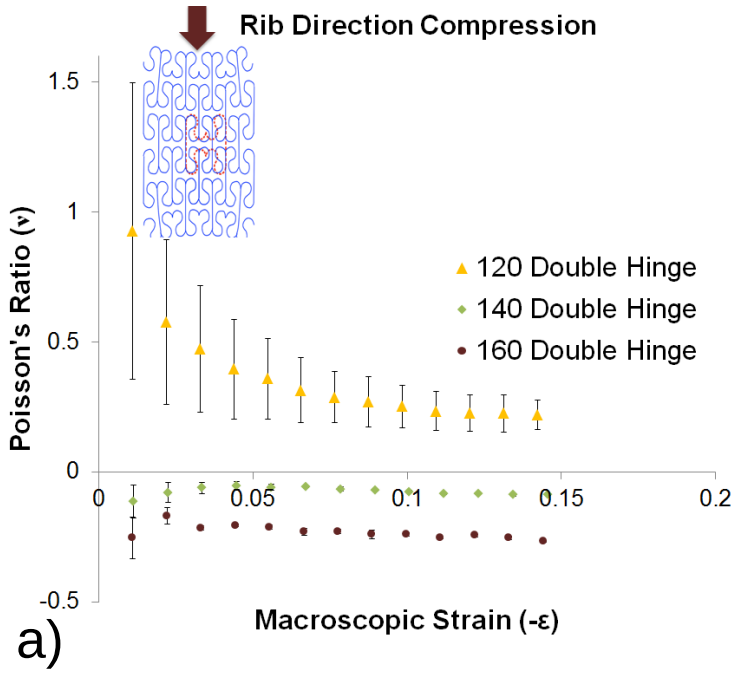

Figure S8. Poisson's ratios. a) Poisson's ratio can be tuned by changing s-hinge arc angle. Experimental Poisson's ratios when compressed along the rib direction**.**

1.3 Latch Design

Several designs were tested for the auxetic unit cell to see which holds and releases the latch the best. Because this auxetic latch is one single connected unit, there are several challenges in designing a proper latch; this is because as the arrow is pushed downwards, the forces travel through the body of the hinge and separate the bottom holding rods. To address this problem, we tried to make an attachment bar at the bottom and changed the length of the holding rod to prevent rod separation. Ultimately, we settled on a design that included a greater thickness at the bottom to address this problem (Main text Figure 5e). In this design, a rounded base was included where the arrow joins the auxetic unit in order to minimize strain at that point.

Supplemental Movies

Movie S1 shows the deformation of the 225-degree arc angle s-hinged auxetic printed in white PLA filament when deformed along the rigid ribs in uniaxial compression testing.

Movie S2 shows the deformation of the 225-degree arc angle s-hinged auxetic printed in white PLA filament when deformed along the hinges in uniaxial compression testing.

Movie S3 shows the bistability of the 140-degree arc angle s-hinge unit cell printed in black PLA filament when deformed along the hinge direction in uniaxial compression testing.

Movie S4 shows the non-auxetic and auxetic properties of the original and modified Batman.

Movie S5 shows latching of the structure in Fig. 5e, and unlatching by transverse pulling.